Radio tracking of the interplanetary coronal mass ejection driven shock crossed by Ulysses on 10 May 2001

S. Hoang,[1] C. Lacombe,[1] R. J. MacDowall,[2] and G. Thejappa[3]

Received 9 June 2006; revised 17 May 2007; accepted 24 May 2007; published 8 September 2007.

[1] We report on the detection of type II radio emission which was observed for more than a day prior to the arrival of an interplanetary shock at Ulysses. We use local spectral emission peaks, computerized from time-averaged intensity spectra of the type II burst, to track the associated emitting shock. In the spectrogram plotted as a function of time and inverse frequency, these peaks appear as elongated clusters of data points, organized in fundamental-harmonic bands and delineating drifting emission features. Least squares linear fittings to identified clusters give straight traces with different slopes. Most of these, when extrapolated to the Sun, are found to converge nearly at the same starting time, allowing determination of the average shock speed. Shortly before the shock crossing, intense Langmuir waves were detected at the electron plasma frequency upstream of the shock. This plasma wave enhancement together with the radio emission observed predominantly at the harmonic of the plasma frequency, all point to the occurrence of the type II radio source region in the upstream electron foreshock. We have accurately substracted the thermal noise background from the observed emission intensity to deduce the type II brightness temperatures at the fundamental and harmonic near the shock crossing. The measured brightness temperature of the type II harmonic emission is found to peak at a value of $\simeq 3 \times 10^{13}$ K just after the shock crossing; just before, the harmonic brightness temperature is $\simeq 10^{12}$ K and the fundamental brightness temperature $\simeq 8 \times 10^{11}$ K.

Citation: Hoang, S., C. Lacombe, R. J. MacDowall, and G. Thejappa (2007), Radio tracking of the interplanetary coronal mass ejection driven shock crossed by Ulysses on 10 May 2001, *J. Geophys. Res.*, *112*, A09102, doi:10.1029/2006JA011906.

1. Introduction

[2] It is generally accepted that solar type II radio bursts observed at hectometer and kilometer wavelengths in the interplanetary medium (IPM) are due to electrons accelerated in the vicinity of shocks driven by IP coronal mass ejections (CMEs) [e.g., *Bougeret*, 1997, and references therein]. These emissions are observed as patchy narrow-frequency bands drifting slowly from high to low frequencies. The gradual frequency drift is due to the progression of the emitting shock moving outward from the Sun through the corona into regions of decreasing plasma densities n_e in the IPM. In some rare cases, two harmonic bands of emission can be observed, suggesting that the type II radio emission is generated by plasma radiation processes at the electron plasma frequency f_p (kHz) $\simeq 9 n_e^{1/2}$ (cm^{-3}) and its second harmonic $2f_p$, with highly variable intensities.

[3] Most of the time, these emissions have been observed remotely in the IPM with very weak intensities, often of the order of the local plasma quasi-thermal noise (QTN) [*Meyer-Vernet et al.*, 2000]. Very few cases, however, have been reported where they can be followed throughout the IPM until the shock arrival at the spacecraft (s/c). The observation by the Ulysses s/c of the CME driven shock on 10 May 2001 constitutes one such exception. Another case was previously reported by *Reiner* [2000] to be observed by the Wind s/c on 26 August 1998. *Bale et al.* [1999] studied the source region of that type II radio burst, using electron data measured on board Wind; from these observations, they could infer some large-scale shock structure in the source region upstream of the shock. *Knock et al.* [2001] applied and refined the stochastic growth theory (SGT) to that type II burst, to interpret the flux densities they deduced from the dynamic spectrum of data observed by *Reiner* [2000].

[4] In this paper, we shall concentrate on the case, unique up to now on Ulysses, of the IP CME driven shock observed on 10 May 2001. This shock could be tracked by the type II radio burst until the shock arrival at the s/c and, later on, in the downstream region. In section 2 we describe the observations and the radio instrument used on Ulysses. In section 3 we present the data analysis in several

[1]Laboratoire d'Etudes Spatiales et d'Instrumentation en Astrophysique, Observatoire de Paris, Meudon, France.
[2]NASA Goddard Space Flight Center, Greenbelt, Maryland, USA.
[3]Department of Astronomy, University of Maryland, College Park, Maryland, USA.

Copyright 2007 by the American Geophysical Union.
0148-0227/07/2006JA011906

aspects. (1) We begin with our method of clustering spectral emission peaks of the type II along the shock progression, to derive new physical insights about the radio source regions of the type II burst along the shock front. (2) We show the close relation that exists between the observed emission frequency and corotating plasma density structures encountered by the shock. (3) We then give the map of the radio sources distributed along the shock front that are responsible for the drifting emission bands observed remotely at the s/c. Section 4 presents a time series of radio spectra observed along the shock approach and used to investigate the shock structure and type II radio emission mechanism. In section 5, we deduce some characteristics about the local structure of the emitting shock. Section 6 gives the radio flux density and brightness temperature of the type II together with the local plasma frequency measured by the radio receiver along the shock crossing path. Finally, in section 7, we give a summary and conclusion.

2. Observations

[5] We use the data from the Radio Astronomy Receiver (RAR) on the Ulysses Unified Radio and Plasma Wave (URAP) Experiment [*Stone et al.*, 1992]. The RAR measures the wave electric fields in two bands. The high-band receivers consist of 12 discrete channels of 3 kHz bandwidth, approximately logarithmically spaced between 52 and 940 kHz and nonlinearly swept in 144 s. The low-band receivers cover the range from 1.25 to 48.50 kHz with 64 channels of 0.75 kHz bandwidth, which are linearly spaced and swept in 128 s. During the period including the present observations, one of the high-band receivers, the HIGH S-receiver, was connected to both the spin-axis electric monopole of 7.5 m and the spin-plane thin strip electric dipole of 2 × 35 m (electrical length h = 35 m), which were configured in the summation mode for direction finding purposes [*Manning and Fainberg*, 1980]. In the low band, one of the receivers, the LOW S-receiver, was connected to the spin plane dipole alone for the purpose of properly measuring the plasma QTN background [*Meyer-Vernet et al.*, 2000] and several other weak emissions like the type II burst under consideration.

[6] Figure 1 displays the radio spectrogram observed from 7 to 10 May 2001 in the 10–1000 kHz range, using both the LOW and HIGH S-receivers. The intensity of the measured radio emission relative to background is plotted as a function of time t and frequency f and coded with a gray scale in units of dB above background. The background at f is defined as the lowest 1% of the data within the whole 4-day interval of observation. This intensity representation is particularly well suited for weak signals like type II emissions. At frequencies above 10 kHz, the dark, continuous and fluctuating narrow band is the QTN around f_p (the so-called plasma line). In order to trace out frequency drifting emission features and for comparison with Figure 2, local spectral emission peaks obtained from 30-min averaged spectra are also plotted as dot-circles on top of the spectrogram of Figure 1. This will be discussed further in section 3.1 in relation with Figure 2.

[7] In Figure 1, an IP shock can be seen to arrive at the Ulysses s/c on 10 May 2001 ~0036 UT, as evidenced by a sudden jump of f_p from about 15 to 25 kHz, i.e., a change of n_e from about 2.8 to 7.7 cm^{-3}. At that time, Ulysses was at ~1.35 AU heliodistance, −5° heliolatitude, and 106° heliolongitude West of Earth, on its fast descent from the Sun's southern pole to the ecliptic plane. On 7 May after 1200 UT, 3 days prior to this shock arrival, a faint type II emission can be seen drifting from high frequency at 1000 kHz to lower frequencies above ~150 kHz. It thereafter appears weaker or nearly disappears during the day of 8 May. From early 9 May, it appears again and becomes more and more intense at the approach of the IP shock until its passing Ulysses on 10 May at about 1036 UT. Shortly before the shock crossing, intense Langmuir waves are detected in the upstream region as evidenced by large intensity fluctuations near the plasma line. After the shock crossing, Ulysses enters the dense downstream region which accompanies the shock. The plasma density varies considerably, f_p fluctuates and increases up to about 100 kHz, corresponding to n_e = 123 cm^{-3}. The type II harmonic emission band continues to be observed for about 3 hours but only at frequencies higher than the local f_p. This will be described further in section 4.

[8] We searched for the CME which could be associated with the type II emitting shock. Actually two CMEs were reported on 7 May 2001 by the SOHO/LASCO instrument: the first starting at 1006 UT with an initial speed of 600 km/s and the second at 1206 UT with a speed of 1200 km/s. Examination of CME movies from LASCO revealed that these CMEs were both behind the west limb, i.e., in the same solar hemisphere as Ulysses. To determine the heliolongitude of these backsided CMEs at the time of their solar liftoff, we look for a NOAA active region (AR) that could be associated at least with one of them. From the SOHO/MDI magnetogram catalog we found AR 9433 centered at N16 W67 on 29 April 2001, 1106 UT (Solar Geophysical Data, 2001). Assuming that the AR lasts for several days and a solar corotational speed of 13.3° per day, we deduce a heliolongitude of 173° for the AR at the 1006 UT liftoff. Another indication about this AR's location can be found with the group of intense type III bursts starting at high frequency on 7 May at ~0930 UT (Day 7.4), shortly before the CME liftoff at 1006 UT (Day 7.42). At lower frequencies and ~1102 UT (Day 7.46), the leading edge of these type IIIs intersects the local plasma line with production of in situ Langmuir waves, implying that the type III fastest electrons are passing the s/c where the Langmuir waves they produce are detected [*Hoang et al.*, 1994]. By tracing the average Archimedean spiral magnetic field line that guides the type III electrons from the s/c back to the Sun, with its curvature set by the average solar wind speed of 390 km/s measured in situ, we find a value of 195° for the heliolongitude of the spiral footpoint, which is within 22° of the (173°) longitude estimated for the backside AR's center. Further evidence for the backside CMEs was provided by the WAVES radio receiver on the WIND s/c [*Bougeret et al.*, 1995] which observed no type II burst and only groups of complex type III bursts, however with weak intensities and high-frequency cutoff. Again all this points to a backside origin of the AR solar flares associated with the two CMEs.

3. Tracking the Type II Radio Emitting Shock

[9] With the objective of tracking in detail the faint type II radio emission associated with the shock, we use

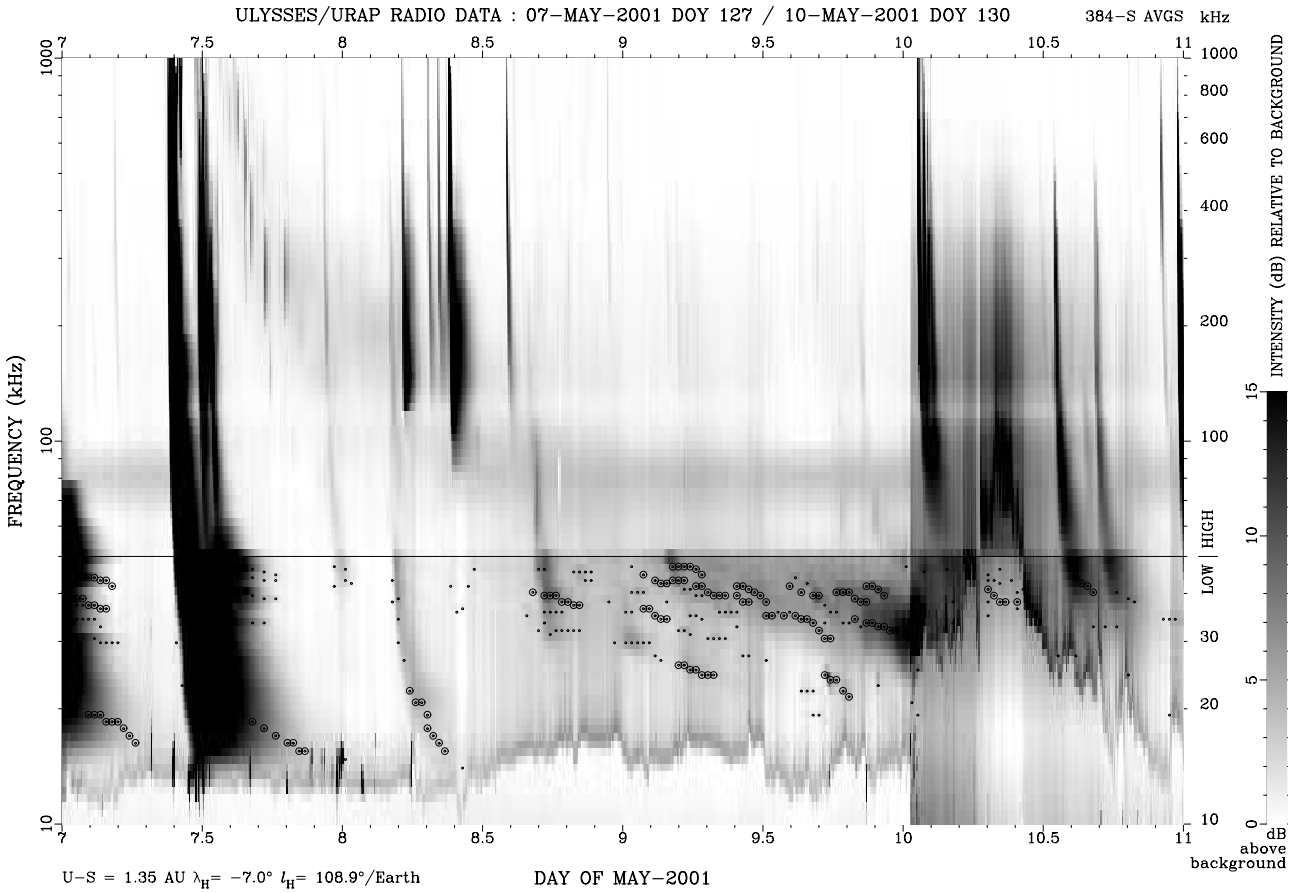

Figure 1. Radio spectrogram observed by Ulysses from 7 to 10 May 2001 in the 10–1000 kHz range, using both the LOW and HIGH BAND S-receivers. The intensity relative to background is plotted in the standard format as a function of time and frequency and coded with a gray scale in units of dB above background. Above 10 kHz the quasi-thermal plasma line is the band of fluctuating intensity and frequency. The arrival of an interplanetary shock at Ulysses on 10 May 2001 at 0036 produces a sudden jump of the plasma line from ~15 to 30 kHz, followed by a large variation of the plasma frequency up to ~100 kHz during about 1 day. Type II emission is seen as patchy narrow-frequency bands drifting slowly from high to low frequencies, predominantly in the low-frequency band, until and shortly after the shock passage. More rapidly drifting features are type III bursts. Local spectral emission peaks obtained from 30-min averaged spectra are plotted as dot circles on top of the spectrogram to trace out drifting emission features.

data from the low-band S-receiver chosen for its high frequency resolution and sensitivity. (The reason for a high sensitivity in the low band is that there is no dominating noise contribution from the short Z spin-axis monopole which is usually connected to the high-band receiver for the direction finding.)

[10] To conveniently visualize the progression of the radio emitting shock in the IPM, Figure 2 displays the spectrogram of Figure 1 with the new ordinate $1/f$. The choice of the inverse of the emission frequency $1/f$ stems from the fact that in the IPM n_e varies with heliodistance r approximately as r^{-2}, so f_p as $1/r$ [e.g., *McComas et al.*, 1992; *Issautier et al.*, 1998]; therefore $1/f$, which is proportional to $1/f_p$ in the plasma radiation hypothesis, scales as r. (For comparison, r is given in AU together with f in kHz on the right vertical axis of the figure using an average f_p of 20 kHz at 1 AU.) This property has been widely employed with success to study IP solar radio bursts [e.g., *Kellogg*, 1980; *Hoang et al.*, 1994; *Poquérusse et al.*, 1996; *Reiner et al.*, 1998a, 1998b; *Dulk et al.*, 1999].

3.1. Clustering Spectral Emission Peaks

[11] As the result of using $1/f$ as the ordinate in Figure 2, many drifting emission features appear now as straight traces of irregular and intermittent blobs with different slopes. In order to disentangle these patchy emission "clouds" along different traces and computerize their identification, a computer code is first used to characterize all local spectral emission peaks (time, frequency, intensity) that appear in successive 30-min averaged spectra (which correspond to vertical cuts through the spectrogram). The resulting emission peaks at t and f are plotted as dots on top of the spectrogram. They delineate many elongated clusters of points with different slopes, tracing the type II burst we study and other drifting emissions like type III bursts. The

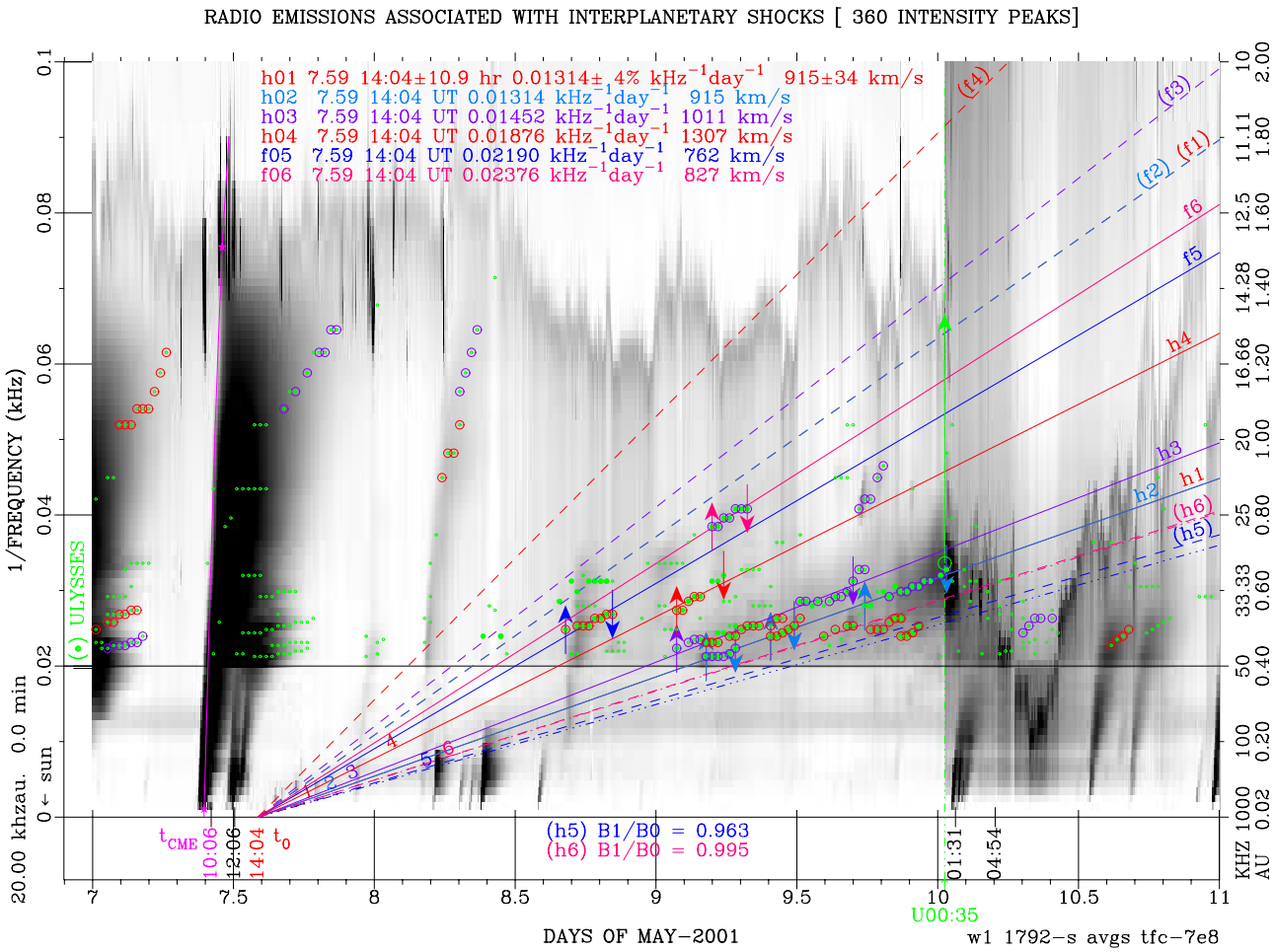

Figure 2. Nonstandard radio spectrogram plotted in the $t - 1/f$ coordinates for the same data and interval as Figure 1. Shock crossing at Ulysses (with time in format Uhhmm) indicated by the green dash-dot vertical line and f_p jump arrow. Local spectral emission peaks obtained from 30-min averaged spectra are plotted (green dots) on top of the spectrogram. They delineate many elongated clusters of points with moderate positive slopes, highlighting the type II burst associated with the shock. Identified clusters (circles surrounding thick dots) are bracketed by two arrows, directed respectively upward (beginning of cluster) and downward (end). Straight-line fits to these clusters are plotted as solid lines assuming the radiation mode at fundamental (f) or harmonic (h); predicted lines for the other mode are plotted as dashed lines. The cluster lines converge at the Sun to the same time t_0; positive shift from the CME liftoff t_{CME} indicates shock acceleration (see text). (top insert) The t_0, slope and shock speed for cluster lines fitted ($h01 - f06$); the shock speed is deduced from the measured slope assuming the quantity $(f_p r)_0 \simeq 20$ kHzAU in the source.

latter can be easily recognized because of their much steeper slopes due to their faster frequency drift rates.

[12] A second computer code is next applied to identify these elongated clusters and subsequently to filter out undesired or unidentified isolated peaks, interferences, or artefacts. The identification is based on the following criteria. (1) Each identified cluster must be along a trace of positive slope. (2) It must contain at least p consecutive peaks that should not be separated by more than dt in time. (3) It must contain at least n consecutive frequencies that should not be separated by more than df in frequency. (4) The number of peaks at the same frequency in a cluster should not exceed the specified maximum number m (in order to eliminate parasite peaks occurring at the same frequency). The clusters thus identified with $p = 4$, $n = 3$, $m = 4$, and $dt = 0.05$ day, $df = 1.50$ kHz, are plotted in Figure 2 as circles surrounding dots which represent the local spectral peaks detected systematically by the first computer code.

3.2. Fitting the Type II Elongated Cluster Lines

[13] In order to highlight the radio link between the CME at the Sun and the shock at Ulysses, we shall try now to group together those clusters which are likely to be related to the type II emission generated from the shock. For that purpose, we select (by hand in this study) those clusters with positive slopes ranging from small to moderate values that appear to converge at the Sun to nearly the same time t_0 about the CME liftoff. We first concentrate on the 3 clusters of approximately the same slope which lie along the line

labelled $h1$ just before the shock passage at Ulysses on 10 May 2001 at 0035:55 UT (day 10.025), as can be seen in Figure 2. A straight-line fit to the three clusters in the $t - 1/f$ coordinates leads to the line $h1$ expressed by

$$\frac{1}{f} = A + B \times t, \tag{1}$$

with $A = -0.100 \pm 5\%$, $B = 0.013 \pm 4\%$ and a correlation coefficient R of 0.996 for 23 fitted data points. This number of points differs slightly (by 15%) from the total number of peaks (circles) in the three clusters. This is due to the fact that some of the clustered peaks are rejected because their deviation from the straight line is larger than the average, while other peaks are added (thick dots) because they lie around the line within the average deviation. The final groups of consecutive peaks retained for the fit are shown in Figure 2 as bracketed each by two arrows directed upward (start of group) and downward (end of group).

[14] Here $h1$ extrapolates at $1/f = 0$ toward a time $t_0 = -A/B = 7.59 \pm 0.45$, corresponding to 1404 UT ±10.9 hours on 7 May. The uncertainty δt_0 on t_0 results from the fitting uncertainties δA and δB, respectively, on A and B. To see the role of the starting time t_0 for other elongated clusters, we shall consider later in Figure 2, we first test the coordinate transformation by taking the origin of time at t_0 = 1404 UT found above for $h1$. Then constraining the cluster line $h1$ to pass t_0 at $1/f = 0$ and adjusting it to the same data points in the new coordinate system will result in the newly fitted line, labelled $h2$, with $A = -0.100$, $B = 0.013$ and $R = 0.996$, which remain unchanged as expected.

[15] Applying the same linear fitting (equation (1)) as for $h1$ to the cluster line $h3$ leads to the results: $A = -0.100 \pm 9\%$, $B = 0.013 \pm 7\%$, $R = 0.981$, and $t_0 = -A/B = 1038$ UT ±18.5 hours, for 22 fitted peaks. The uncertainties δA, δB, and δt_0 are about two times larger than those found for $h1$ with about the same number of data points but observed over a time interval shorter (0.6 day) than for $h1$ (0.9 day). Applying the same fitting procedure to the rest of identified cluster lines, $h4$, $f5$, and $f6$, with a much lesser number of peaks (8, 8, and 7, respectively) spanning a much shorter time interval (0.17, 0.17, and 0.12 day, respectively) results in values for t_0 of 0317, 1918 and 1138 UT, respectively, on 7 May 2001. The uncertainties δt_0 found are excessively large, amounting to 56, 91, and more than 100 hours, respectively.

[16] From the above, we may not consider the start time t_0 found for small clusters to be representative of the departure of the type II emitting shock from the Sun. Instead, we shall choose the start time t_0 found for the most compact and longest cluster line $h1/h2$ to represent the common start time for all the cluster lines $h1/h2$ to $f6$. In this representation, the CME driven shock is considered to start emitting the type II burst at some distance from the Sun and then to propagate radially at constant speed in the IPM until its passage at Ulysses. In Figure 2, all the cluster lines seem to start from the Sun nearly at the same time t_0 of $h1/h2$. This view corresponds actually to a shock propagating radially at constant speed and emitting the type II radio emission along the shock front.

[17] Therefore we shall perform the same treatment we have just applied to $h2$, with t_0 of $h1$ taken as the common departure time, to other identified elongated clusters that show up in Figure 2 as originating from t_0 at $1/f = 0$. This leads to the fitted cluster lines labelled $h3$ and $h4$ (harmonic), $f5$ and $f6$ (fundamental), and plotted as solid lines in Figure 2, as will be discussed further in the following section.

3.3. Slope and Radiation Mode of the Cluster Line

[18] The slope B of an elongated cluster line fitted above can be written in the form

$$B = \frac{d(1/f)}{dt} = \frac{\cos\theta}{a(f_p r)_0} \times V_{sh}, \tag{2}$$

where a is the radiation mode (nominally equal to 1 for F, 2 for H), $V_{sh} = dr/dt$ is the shock speed, and θ the angle between the shock velocity and IP radial density gradient ($\theta = 0$ for radial propagation); $(f_p r)_0$ is the constant of proportionality in the plasma density distribution in the IPM assumed to vary as $f_p r = (f_p r)_0$ along the IP Archimedian spiral plasma structure that passes the type II source at the shock front. $(f_p r)_0$ can be fixed by the knowledge of f_{p0} at a given heliodistance r_0, e.g., at the s/c or radio source passed by the plasma density structure.

[19] The slope B varies as the inverse of the radiation mode a. Therefore assuming the radiation mode for a fitted line (plotted as a solid line) to be harmonic (h) or fundamental (f), we can deduce the emission line for the other mode (plotted as a dashed line) by multiplying the slope of the fitted line by 2 or 1/2. The fitted cluster line $h1/h2$ is known to be harmonic (h) since, at the shock crossing, it passes through about twice the upstream plasma frequency f_{pu}. So the other mode at the fundamental (f) is deduced by multiplying the slope B of $h1/h2$ by 2 and shown in Figure 2 as the dashed line labelled $(f1)/(f2)$ which departs from the Sun at the same t_0. It is noteworthy that in contrast to the harmonic $h1/h2$, the predicted fundamental $(f1)/(f2)$ does not cross any identified cluster along. For similarity with the harmonic line $h1/h2$, the nearby cluster lines $h3$ and $h4$ are fitted assuming harmonic emission, with their extrapolated fundamental lines ($f3$) and ($f4$) plotted as dashed lines. As noted for $(f1)/(f2)$, there exist no identified clusters along ($f3$) and ($f4$). The sole cluster lines, labelled $f5$ and $f6$ and plotted as solid lines in Figure 2, are fitted to identified clusters assuming fundamental radiation. The reason for this assumption is that the extrapolated harmonic lines ($h5$) and ($h6$), plotted as dashed lines in Figure 2, do pass through at least one identified cluster in accordance with the fundamental-harmonic radiation hypothesis. Indeed, the predicted lines ($h5$) and ($h6$) can be fitted to the nearby clusters by the same procedure, resulting in the fitted (dotted-dashed) lines which lie very close to the predicted (dashed) lines, with the ratios of the fitted to predicted slopes respectively of 0.963 and 0.995. In fact, in this case, we may instead start fitting the harmonic lines and then deduce the predicted fundamental ones as well.

[20] As noted above, all the predicted fundamental lines have encountered no identified clusters. In other words, most of the identified clusters of the type II burst have been found at harmonic. This scarcity of observing the type II fundamental component in the IPM may be explained by

the masking effect of the ubiquitous QTN on radio emission at frequencies near the local f_p. It may also be due to an occultation of these fundamental emission frequencies by overdensities present between the emitting region and the receiver; this will appear clearer in section 3.5.

3.4. Shock Speed and Plasma Frequency Along the Cluster Line

[21] As can be seen from Figure 2, the common departure time t_0 at 1404 UT of the type II cluster lines deviates significantly from the time of the CME at 1006 UT. This 4-hour lag could be interpreted as the result of an acceleration of the CME driven shock at some heliodistance in the IPM. Indeed, the CME was observed by the SOHO/LASCO instrument to leave the Sun with a speed of 600 km/s, which is significantly lower than the shock transit speed V_T of 964 km/s computed from the transit time between t_0 and the passage of the shock at Ulysses on 10 May 2001 at 1036 UT. Assuming the shock propagates radially in a steady medium, from equation (2) we can see that a shock acceleration will produce an increase of the slope B of a cluster line and hence a positive shift of t_0 from the CME liftoff time; and conversely, a speed decrease (deceleration) will produce a decrease of B and hence a negative shift of t_0 from the time of the CME. (At this point, it is worth noticing that a shock moving with a constant speed through different densities along its front will produce elongated clusters of different slopes which would all converge at $1/f = 0$ to the time of the associated CME.) As a crude estimate of the heliodistance r_0 at which the type II shock starts accelerating, we consider a cluster line, e.g., h1/h2, departing from $1/f = 0$ at t_0 with a slope B, and a hypothetical line starting from the Sun at the time of the CME with a slope equal to $B \times (600/964)$. The intersection between these lines gives $r_0 \simeq 0.1$ AU.

[22] Until now, we have derived V_T from the departure time t_0 and shock passage, independently of any knowledge on the radiation mode. On the other hand, from equation (2) we may also derive the shock speed V_{sh} from the measured slope B, knowing the radiation mode a and the local f_p times distance r at the source, $(f_p r)_0$. This is actually the case for the fitted harmonic line h1/h2 which has been observed to pass through the local $2f_{pu}$ at the shock crossing. Thus using $(f_p r)_0 \simeq 20$ kHzAU and a = 2 (nominal value for harmonic) yields $V_{sh} = 915$ km/s, as indicated in the top inset of Figure 2. In fact, the frequencies of the peaks detected at harmonic bands are rather somewhat higher than the local $2f_p$. (Further consideration will be given in the next section.) So using $a \simeq 2.1$ results in $V_{sh} = 960$ km/s, a value very close to $V_T = 964$ km/s as should be expected.

[23] At the shock crossing, the shock front speed V_C can be estimated by using the Rankine-Hugoniot equation of conservation of mass

$$(V_C - V_u) \times n_{eu} = (V_C - V_d) \times n_{ed}, \tag{3}$$

where $n_{eu} = 2.7$ cm^{-3} and $n_{ed} = 7.4$ cm^{-3} are the upstream and downstream densities (see section 4), and $V_u = 377$ and $V_d = 706$ km/s the measured upstream and downstream solar wind velocities [*Bame et al.*, 1992], assumed to be aligned with the shock normal. We obtain $V_C = 893$ km/s, which is compatible with the speed values (960 and 964 km/s) found above.

3.5. Type II Source and Plasma Frequency Along the Shock Front

[24] In Figure 2 the cluster lines of the type II burst, which converge to the same starting point ($t = t_0$, $1/f = 0$) and exhibit different slopes B, could be considered to be due to emissions from radio sources produced by the shock front moving radially with constant speed V_T, across various density structures which corotate with the Sun. From equation (2) we can see that an increase (decrease) of the slope B, which varies as the inverse of $(f_p r)_0$ in the source, would result from a decrease (increase) in the plasma frequencies (or densities) encountered by the shock at the observing time t_{obs} of the type II. In fact, the average of the quantity $(f_p r)_U$ measured in the IPM by Ulysses from 5 to 9 May 2001 amounts to 19.2 kHzAU with a standard deviation of 11%. On the other hand, the average of the slope B of the 5 harmonic cluster lines, $h1/h2$ to $h6$ (listed in the top inset of Figure 2, with $h5$ and $h6$ deduced from $f5$ and $f6$), is about 0.01385 kHz^{-1} day^{-1} with a standard deviation of 22%. These quantities, $(f_p r)_U$ and B, could be thus considered to vary in reasonable correlation, bearing in mind that the type II emission peak clusters have been observed solely in short time intervals, hence with larger deviations, as compared with the long 5-day interval of continuous measurement of $(f_p r)_U$, resulting thus in smaller deviations.

[25] Therefore in the following, we shall examine the relation foreseen above in further detail by comparing the quantity $(f_p r)_0$ of each fitted type II cluster line with corotating 30-min averages of the quantity $(f_p r)_U$ measured at Ulysses. To derive $(f_p r)_0$ from the fitted slope B of each cluster line in equation (2), we assume the shock propagates radially with a constant speed $V_T = 964$ km/s and the radiation mode $a = 1$ for the fundamental F, 2 for the harmonic H. The corotating $(f_p r)_U$ measured at Ulysses on a spiral plasma density structure is traced back to the Sun to intersect the shock front at the time of the observed type II, using an average solar wind speed of 390 km/s and a solar corotational speed of 14.1° per day as seen from Ulysses.

[26] For illustration, Figure 3 (top) presents a schematic diagram of the 2-D geometry of the CME-driven shock propagating radially from the Sun to Ulysses, at the shock passage on 10 May 2001 at 0036 UT. The shock is assumed to be spherical in shape and centered on the flare/AR-9433 at 173°W. During the interval of observation from 7 to 10 May 2001, Ulysses was near the ecliptic plane at heliolongitude from 110 to 106° west of Earth. Therefore the center of the CME/shock was about 65° of heliolongitude West of Ulysses, a situation favorable to observe the shock nearly in a spherical shape and without strong interactions from the driving CME with the solar wind upstream when observed ahead or East of the CME [e.g., *Cane*, 2000, and references therein]. Thus we may assume the corotating $(f_p r)_U$ data measured at Ulysses remain unchanged, i.e., with negligible radial evolution, when traced back to the Sun at the encounter with the shock. This allows relating the plasma frequency upstream of the shock to that measured at Ulysses stationed farther in the solar wind, as described in detail by *Lengyel-Frey* [1992].

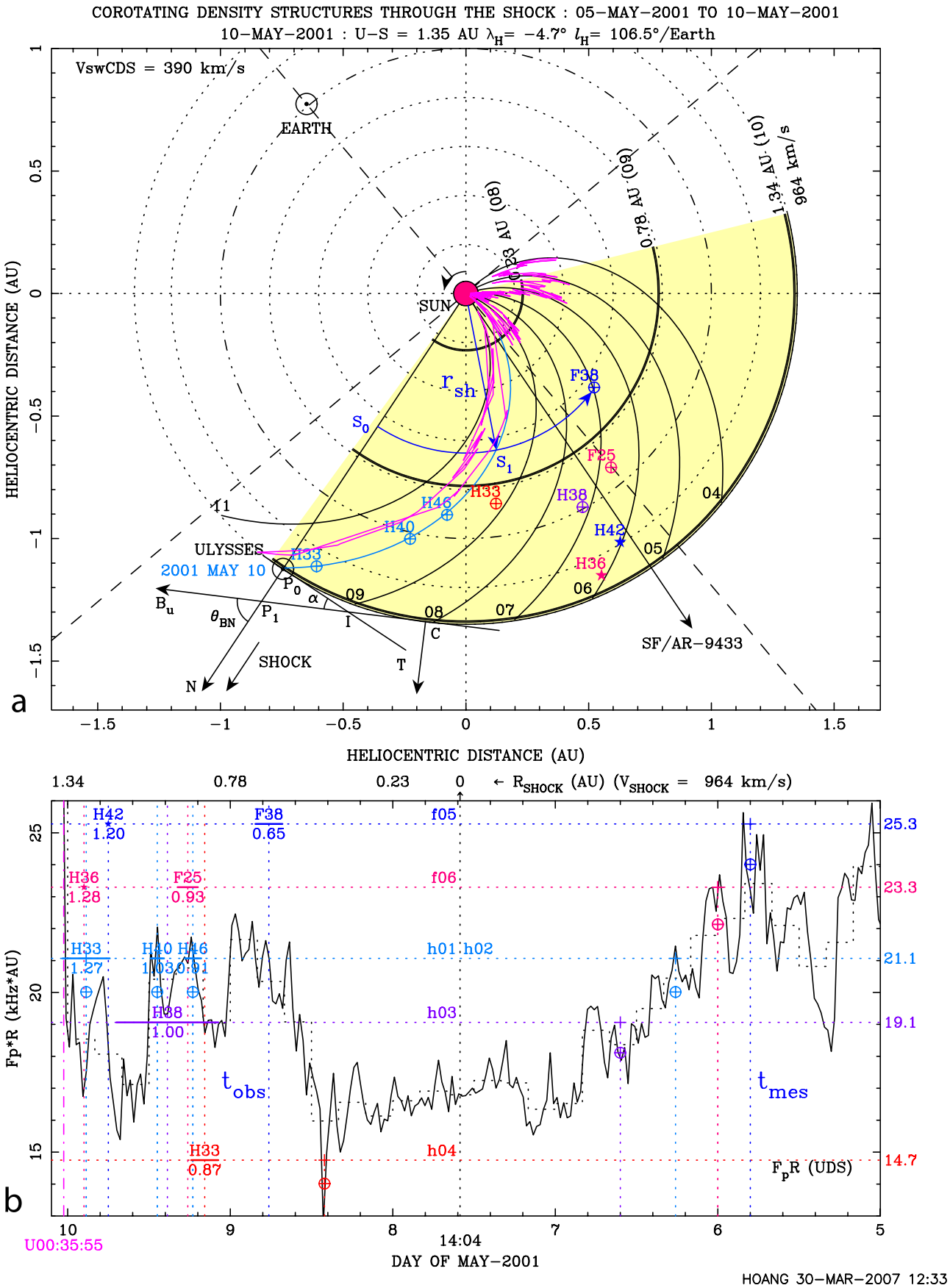
COROTATING DENSITY STRUCTURES THROUGH THE SHOCK : 05-MAY-2001 TO 10-MAY-2001
10-MAY-2001 : U-S = 1.35 AU λH= -4.7° lH= 106.5°/Earth
VswCDS = 390 km/s
EARTH
SUN
0.23 AU (08)
0.78 AU (09)
1.34 AU (10)
964 km/s
r sh
S0
S1
F38
F25
H33
H38
H46
H40
H42
H36
ULYSSES
2001 MAY 10
P0
P1
α
I
C
T
N
Bu
θBN
SHOCK
SF/AR-9433
11
09
08
07
06
05
04
HELIOCENTRIC DISTANCE (AU)
a
1.34
0.78
0.23
0
← RSHOCK (AU) (VSHOCK = 964 km/s)
H42 1.20
F38 0.65
f05
H36 1.28
F25 0.93
f06
H33 1.27
H40 1.03
H46 0.91
h01 h02
H38 1.00
h03
H33 0.87
h04
tobs
tmes
FpR (UDS)
25.3
23.3
21.1
19.1
14.7
Fp*R (kHz*AU)
b
U00:35:55
14:04
DAY OF MAY-2001
HOANG 30-MAR-2007 12:33

Figure 3

[27] In order to highlight the relation between the type II emitting shock and the upstream solar wind plasma frequencies (densities), Figure 3 (top) displays different spirals passing Ulysses on several days encompassing the type II observation interval, together with the time series of the corotating 30-min averaged $(f_p r)_U$ data (pink lines) measured at Ulysses. Figure 3 (bottom) presents the same $(f_p r)_U$ time series data, plotted (continuous line) as a function of time from 5 to 10 May 2001. In the same figure, the values of $(f_p r)_0$ at the type II sources deduced from the 5 fitted cluster lines of Figure 2 are also plotted as functions of the observing time (at midcluster) and represented by thick segments lying on horizontal dotted lines, labelled *h*01/*h*02, *h*03, *h*04, *f*05, and *f*06 as in Figure 2. (The ends of each segment correspond to the start and end of each identified cluster bracketed by two arrows directed respectively upward and downward in Figure 2.)

[28] Assuming the source region of the type II to lie near the shock front, the heliodistance of the shock front at the time t_{obs} of the observed type II may be given by

$$r_{sh}(t_{obs}) = V_T \times (t_{obs} - t_0), \tag{4}$$

where t_0 is the common departure time of the type II cluster lines (Figure 2). Here r_{sh} is indicated in AU on the top of Figure 3b and below each segment of identified clusters. Above each segment are also indicated the radiation mode (*F* or *H*) and frequency (kHz) of the observed type II; e.g., *F*38 means 38 kHz at fundamental (line *f*05), and *F*25 means 25 kHz at fundamental (line *f*06). For predicted (extrapolated) values, the segments are replaced by stars; e.g., *H*42 above the star means predicted harmonic at 42 kHz on line *f*05.

3.6. Density Structures in the Type II Source Regions

[29] We try now to determine which corotating densities $(f_p r)_U$ measured continuously at Ulysses correspond to the $(f_p r)_0$ densities in the source regions as deduced from the different cluster lines, h01/h02 to f06. Referring to Figure 3b, we search for the $(f_p r)_U$ data that lie closest to the $(f_p r)_0$ data of each considered cluster line. The time t_{mes} of each $(f_p r)_U$ value thus found is indicated by a vertical dotted line which intersects its associated cluster line, *h*01/*h*02 to *f*06 (plotted as horizontal dotted line), at a point marked by a plus symbol. Since the observed frequency *f* at *F*(*H*) is in general found to be somewhat higher than the local f_p ($2f_p$) in the emission source, Figure 3b shows the source locations plotted as circled plus symbols which are obtained using $f = 1.05(2.10) \times f_p$ for *F*(*H*) emission. As a result, they appear to be quite compatible with their associated $(f_p r)_U$ values.

[30] From Figure 3b, we can see that several $(f_p r)_0$ densities in type II source regions are small-scale overdense blobs as revealed by the $(f_p r)_U$ data measured earlier at Ulysses; e.g., the density blobs shown by circled plus symbols associated with the cluster lines *f*05 and *f*06, for the sources *F*38–*H*42 and *F*25–*H*36, respectively. It is worth noticing that the two fundamental emission sources, *F*38 and *F*25, observed at $t_{obs} \sim 8.8$ and 9.2, respectively, come from the highest density flows which passed Ulysses 3 days earlier, at $t_{mes} \sim 5.8$ and 6.0, respectively. This explains why these fundamental emissions could be seen by the radio receiver on Ulysses since the s/c was then in a lower density path than the emitting regions. Their harmonic counterparts, *H*76 and *H*50, were not observed simply because they were out of the low-frequency receiver range (1.25 to 48.50 kHz). Later on, however, the harmonic emissions *H*42 and *H*36 produced by the same source regions at $t_{obs} \sim 9.75$ and 9.9, respectively, could be again observed within the receiver frequency range. At the other extreme, the harmonic emission *H*33 (kHz) identified on the cluster line *h*04, and observed on day ~9.2, appears to originate from the lowest density structure passing Ulysses at $t_{mes} \sim 8.42$. It is clear then that its *F* counterpart could not be seen by Ulysses, since the high density path existing between the source and the s/c should block the fundamental radiation coming from lower plasma densities. These low densities in the source explain also why the cluster line *h*4, as shown in Figure 2, exhibits the highest slope among the identified harmonic emission clusters (see equation (2), section 3.3).

3.7. Mapping the Type II Radio Sources Along the Shock Front

[31] In this section, referring to Figure 3a, we shall represent the observed type II sources in a 2-D heliocentric map centered on the Sun-Ulysses line and assumed to coincide with ecliptic plane (Ulysses was near this plane). The location of each radio source along the moving shock front at the observing time t_{obs} can be defined by the shock heliodistance $r_{sh}(t_{obs})$ (equation (4), section 3.5) and by the source heliolongitude as referred to the Sun-Ulysses line.

[32] As an example, we consider the source *F*38 observed from Ulysses at $t_{obs} \sim 8.76$ and found on the shock front at heliodistance $r_{sh} \sim 0.65$ AU. Its heliolongitude with respect to Ulysses can be defined as

$$l(F38) = \widehat{S_0 S_1} + \widehat{S_1 F38}, \tag{5}$$

Figure 3. (a) Schematic diagram of the 2-D geometry of the CME shock at its passage at Ulysses on 10 May 2001 at 0036 UT, propagating radially (circles) from the Sun to Ulysses and centered on the associated flare/AR-9433 at 173°W of Earth. Different interplanetary Archimedian spirals (constructed with V_{sw} = 390 km/s) passing Ulysses between 4 and 11 May are plotted, together with corotating 30-min averaged $(f_p r)_U$ data measured at Ulysses (pink lines). Observed type II source regions at the shock front, deduced from the fitted cluster lines of Figure 2 and Figure 3b, are plotted as a circled plus symbol (fitted clusters) and star (extrapolated); e.g., *F*38 means 38 kHz at Fundamental and *H*42, 42 kHz at Harmonic. (b) Values of $(f_p r)_0$ of the type II sources, deduced from the fitted cluster lines *h*01/*h*02 to *f*06, plotted at different times of observation at midcluster as thick segments (star) for fitted clusters (extrapolated). The 30-min averaged $(f_p r)_U$ data measured at Ulysses are plotted as continuous line versus time. The times of the $(f_p r)_U$ values which lie closest to different $(f_p r)_0$ values of fitted clusters are indicated by vertical dotted lines which pass through points shown by a plus symbol and a circled plus symbol in the density structures $(f_p r)_U$ associated with the type II sources (see text for further detail).

where $\widehat{S_0S_1}$ is the longitude of point S_1 at r_{sh} on the density flow spiral that passes through Ulysses at t_{obs}; $\widehat{S_1F38}$ is the source longitude increase due to the corotating density flow moving from $t_{obs} \sim 8.76$ days to $t_{mes} \sim 5.8$ days and given by

$$\widehat{S_1F38} = (t_{obs} - t_{mes}) \times V_{CR}, \tag{6}$$

with V_{CR} = solar corotational speed = 14.1° per day (as seen from Ulysses).

[33] In Figure 3a the source locations thus derived as described above are plotted as circled plus symbols (for fitted cluster lines) and stars (extrapolated cluster lines), together with the radiation mode (F for fundamental, H harmonic) and frequency (kHz). From this map, we may note that in the low frequency range from 20 to 50 kHz, Ulysses has observed the type II radio bursts along a shock front of about 60° longitude extension West of Ulysses and at heliodistance from 0.60 AU outward to the orbit of Ulysses at 1.35 AU. Immediately prior to the shock crossing, the cluster line $h01/h02$ (Figure 3b) passes through the three nearest sources, $H33$, $H40$, and $H46$, lying along the density flow spiral passing through the s/c at the crossing.

4. Radio Spectra Across the Shock

[34] As the shock approaches and overtakes the s/c, the type II radio emission and the local plasma line are observed to change drastically, particularly during the shock crossing. In order to investigate them in detail and with accuracy, we shall use the voltage power spectra measured by the low-band radio receiver at its 128-s full time resolution.

[35] Figure 4 presents typical radio spectra taken successively between 1800 UT on 9 May 2001 and 0400 UT on 10 May 2001. This interval covers the last clusters identified on the line $h1/h2$ of the type II emission prior to the shock crossing (Figure 2). For practical purposes, the voltage power spectrum is measured in V^2 Hz^{-1} at the ports of the receiver. It is averaged over 2-s frequency steps of four data samples and plotted (black dotted lines) as a function of frequency (kHz). To obtain the radio power spectrum at frequencies above the plasma frequency f_p, we have to substract the thermal noise background from the observed power spectrum. The thermal noise is derived by fitting the theoretical quasi-thermal noise spectrum to the observed spectrum [*Meyer-Vernet et al.*, 2000] and plotted as continuous red line. Finally, the power spectrum measured at receiver, V_r^2, is converted to that at the ports of the electric dipole antenna, V_a^2 (which is the physical measure of the radio emission we need to determine the type II brightness temperature as will be explained in section 6) by the relation [*Meyer-Vernet et al.*, 2000]

$$V_a{}^2 = V_r{}^2 \times \left(\frac{C_a + C_b}{C_b}\right)^2, \tag{7}$$

where C_a is the antenna capacitance and C_b the base capacitance of the deployment mechanism and various connection cables between the antenna and receiver [*Manning*, 2000]. V_a^2 is expressed in units of V^2 Hz^{-1} at antenna and plotted as blue dotted lines in Figure 4.

[36] In order to trace out any bursty plasma activity, nonaveraged data are also superposed on observed averaged spectra and plotted in Figure 4 as continuous black lines; these data generally blend together in the absence of nonthermal plasma waves in the observing frequency range.

[37] In Figure 4 the spectral emission peaks identified as the type II burst at harmonic are marked with red circles. They belong to the last cluster identified on the line h1/h2 of Figures 2 and 3. When considering these spectra successively, the type II emission may be seen in different conditions encountered along the shock approach: (1) In the solar wind upstream of the shock, spectra 1 (starting at 2102 on 9 May) to 4 (at 0032 on 10 May). (2) Just before and around the shock crossing, spectrum 5 (10 May at 0034:39). (3) Downstream of the shock, before the radio emission vanishes due to higher densities that occur later on along the s/c path, spectra 6 (10 May at 0036:47) to 10 (10 May at 0319:59).

[38] These spectra show a general increase of the intensity of the type II harmonic emission until the shock crossing at 0035:55 UT on 10 May, and shortly after; thereafter, a general decrease until it disappears in the downstream region. Beside the dominant harmonic emission, a weak fundamental component of the type II emission could be distinguished from spectra 3 and 4 before the shock crossing, and more clearly after thermal background substraction.

[39] The spectrum 5, with its frequency sweep starting from 1.25 kHz at 0034:39 UT, is particularly noteworthy as it spans two interesting observations relating to the shock itself:

[40] 1. Intense Langmuir waves starting just above the local f_p = 14.75 kHz at 0035:13 UT, 42 s before the shock crossing at 0035:55 UT. Their peak amplitude values (continuous black line) are as high as $\sim 10^{-10}$ V^2 Hz^{-1}. Because our 128-s frequency swept receiver can measure one frequency only at a given time (on a 2-s step), it may miss an event occurring at a specific frequency within the sweep, namely f_p, while scanning other frequencies, the exact start time at which the s/c detects the Langmuir waves may be estimated to be between 42 and 42 + 128 = 170 s before 0035:55 UT. At that time (of first detection of Langmuir waves), Ulysses enters the upstream boundary of the electron foreshock, where the solar wind electrons accelerated by the shock drive Langmuir waves at the upstream plasma frequency f_{pu} [e.g., *Filbert and Kellogg*, 1979; *Lacombe et al.*, 1988]; some of their energy is subsequently mode converted to the type II radio emission observed [*Knock et al.*, 2001, and references therein].

[41] 2. An abrupt increase of the spectrum intensity observed between 29.75 and 30.50 kHz at the 0035:55 UT shock crossing. This change is very likely due to the increased thermal noise background that prevails in the dense downstream region of the shock. The exact local f_p in the downstream near the shock crossing is unknown due to the lack of measurement at this time. We may however estimate that value f_{pd} from the intensity jump, using the thermal noise background (red line) fitted before (spectrum 5, f_p = 14.75 kHz) and after the shock crossing (spectrum 6, f_p = 24.50 kHz), and adjusting f_p on the downstream spectrum so as to match the above intensity jump at 30.50 kHz. This gives $f_{pd} \simeq 27.5$ kHz which is very compatible with values of

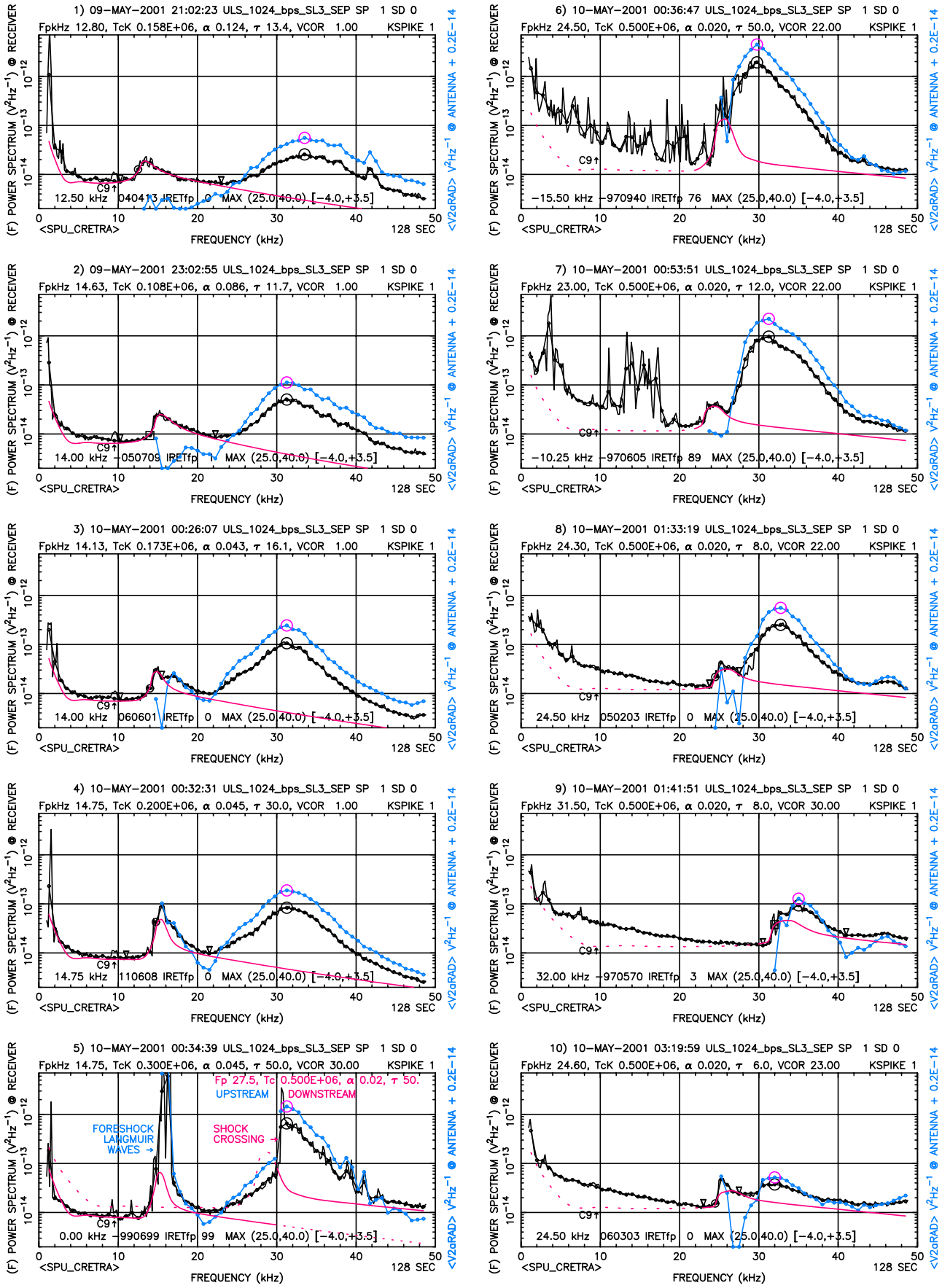
1) 09–MAY–2001 21:02:23 ULS_1024_bps_SL3_SEP SP 1 SD 0
FpkHz 12.80, TcK 0.158E+06, α 0.124, τ 13.4, VCOR 1.00 KSPIKE 1
12.50 kHz 040413 IRETfp 0 MAX (25.0,40.0) [−4.0,+3.5]
2) 09–MAY–2001 23:02:55 ULS_1024_bps_SL3_SEP SP 1 SD 0
FpkHz 14.63, TcK 0.108E+06, α 0.086, τ 11.7, VCOR 1.00 KSPIKE 1
14.00 kHz −050709 IRETfp 1 MAX (25.0,40.0) [−4.0,+3.5]
3) 10–MAY–2001 00:26:07 ULS_1024_bps_SL3_SEP SP 1 SD 0
FpkHz 14.13, TcK 0.173E+06, α 0.043, τ 16.1, VCOR 1.00 KSPIKE 1
14.00 kHz 060601 IRETfp 0 MAX (25.0,40.0) [−4.0,+3.5]
4) 10–MAY–2001 00:32:31 ULS_1024_bps_SL3_SEP SP 1 SD 0
FpkHz 14.75, TcK 0.200E+06, α 0.045, τ 30.0, VCOR 1.00 KSPIKE 1
14.75 kHz 110608 IRETfp 0 MAX (25.0,40.0) [−4.0,+3.5]
5) 10–MAY–2001 00:34:39 ULS_1024_bps_SL3_SEP SP 1 SD 0
FpkHz 14.75, TcK 0.300E+06, α 0.045, τ 50.0, VCOR 30.00 KSPIKE 1
Fp 27.5, Tc 0.500E+06, α 0.02, τ 50.
UPSTREAM
DOWNSTREAM
FORESHOCK LANGMUIR WAVES →
SHOCK CROSSING →
0.00 kHz −990699 IRETfp 99 MAX (25.0,40.0) [−4.0,+3.5]
6) 10–MAY–2001 00:36:47 ULS_1024_bps_SL3_SEP SP 1 SD 0
FpkHz 24.50, TcK 0.500E+06, α 0.020, τ 50.0, VCOR 22.00 KSPIKE 1
−15.50 kHz −970940 IRETfp 76 MAX (25.0,40.0) [−4.0,+3.5]
7) 10–MAY–2001 00:53:51 ULS_1024_bps_SL3_SEP SP 1 SD 0
FpkHz 23.00, TcK 0.500E+06, α 0.020, τ 12.0, VCOR 22.00 KSPIKE 1
−10.25 kHz −970605 IRETfp 89 MAX (25.0,40.0) [−4.0,+3.5]
8) 10–MAY–2001 01:33:19 ULS_1024_bps_SL3_SEP SP 1 SD 0
FpkHz 24.30, TcK 0.500E+06, α 0.020, τ 8.0, VCOR 22.00 KSPIKE 1
24.50 kHz 050203 IRETfp 0 MAX (25.0,40.0) [−4.0,+3.5]
9) 10–MAY–2001 01:41:51 ULS_1024_bps_SL3_SEP SP 1 SD 0
FpkHz 31.50, TcK 0.500E+06, α 0.020, τ 8.0, VCOR 30.00 KSPIKE 1
32.00 kHz −970570 IRETfp 3 MAX (25.0,40.0) [−4.0,+3.5]
10) 10–MAY–2001 03:19:59 ULS_1024_bps_SL3_SEP SP 1 SD 0
FpkHz 24.60, TcK 0.500E+06, α 0.020, τ 6.0, VCOR 23.00 KSPIKE 1
24.50 kHz 060303 IRETfp 0 MAX (25.0,40.0) [−4.0,+3.5]
(F) POWER SPECTRUM (V²Hz⁻¹) @ RECEIVER
<V2aRAD> V²Hz⁻¹ @ ANTENNA + 0.2E−14
FREQUENCY (kHz)
<SPU_CRETRA>
128 SEC
C9↑

Figure 4

f_p downstream of the shock near the crossing. In addition, the rate of the intensity jump could be estimated to be within 0.5 s by analyzing the full resolution data on the 30.50 kHz step (measuring 4 samples in 2 s) of the frequency sweep spanning the shock crossing.

[42] These observations enable us to derive new physical insights on the shock structure as will be described below.

5. Local Structure of the Emitting Shock

[43] We now deduce some key characteristics of the emitting shock around its passage at Ulysses, using radio and magnetic field data measured on board. First we shall ascertain its geometry and then estimate its local curvature and thickness.

5.1. Shock Geometry

[44] To illustrate the geometry of the passage of the shock, Figure 3a shows a schematic drawing of a 2-D slice of the shock around the point of passage P_0, including the upstream magnetic field $\mathbf{B_u}$ tangent to the shock at the contact point C located at some distance from P_0. The shock normal $\mathbf{N}$ is assumed to be radial at P_0 and makes an angle θ_{BN} with $\mathbf{B_u}$. The point P_1, intersection between $\mathbf{N}$ and $\mathbf{B_u}$, represents the passage of Ulysses at the upstream boundary of the electron foreshock, where intense Langmuir waves are detected at least 42 s before the shock crossing, as described in section 4. The tangent $\mathbf{T}$ to the shock at P_0 is shown to intersect $\mathbf{B_u}$ at the point I and angle α.

[45] To derive θ_{BN} at the shock passage on Ulysses (at 0035:55 UT), we use 32-s averaged data of the magnetic field vector $\mathbf{B}$ measured on board [*Balogh et al.*, 1992] in the s/c coordinate system to obtain $\mathbf{B_u} = 6.385(-0.335,0.916,0.219)$ nT upstream, just before (0035:27 UT), and $\mathbf{B_d} = 12.993$ $(-0.323,0.894,0.310)$ nT downstream, just after (0035:59 UT). The shock property of coplanarity of $\mathbf{N}$ with $\mathbf{B_u}$ and $\mathbf{B_d}$ leads to $\theta_{BN} = 79°$, indicating a quasi-perpendicular shock.

5.2. Curvature and Thickness of the Shock

[46] In Figure 3a, for clarity, we have represented the local shape of the shock at P_0 as to be circular and centered on the Sun, and P_0P_1 for $\theta_{BN} \simeq 60°$, well smaller than its value of 79° deduced above. We may get some idea on the shock curvature b which can be defined as

$$b \sim \alpha/P_0C \sim \alpha/2P_0I. \tag{8}$$

Taking

$$P_0I \sim P_0P_1/\tan\alpha \tag{9}$$

yields

$$b \sim \alpha\tan\alpha/2P_0P_1. \tag{10}$$

Finally, using $\alpha = 90° - \theta_{BN} = 11°$, and considering the distance P_0P_1 to be travelled in $\geq$42 s (lower limit set by the uncertainty in detecting an event time with the frequency swept receiver) by the shock at the speed V_T of 964 km/s (section 3.4), yield $b \leq 0.5 \times 10^{-9}$ m^{-1}, which is close to the b value of 10^{-9} m^{-1} deduced by *Knock et al.* [2001] from the observations of *Bale et al.* [1999] of the IP shock crossed by Wind on 26 August 1998.

[47] As an estimate of the shock thickness L_{sh}, we measure the rate of 0.5 s at which the voltage power spectrum jumps at the shock passage (section 4), together with the shock transit speed of 964 km/s as above, to obtain $L_{sh} \simeq 500$ km.

6. Type II Brightness Temperature

[48] In this section we shall derive the flux density and brightness temperature of the type II radio emission, using the full time resolution spectrum data observed and processed between 6 hours prior to the shock passage and 4 hours after, as explained in detail in section 4.

[49] The square spectral electric field E_f^2 of the radio emission is related to the voltage spectral density V_a^2(V^2 Hz^{-1}) measured at the electrically short dipole of electrical length h (with a directivity polar diagram in $2/3 \times \cos^2\theta$), after removal of the thermal noise background (see section 4) [*Manning and Fainberg*, 1980; *Fainberg et al.*, 1985], by

$$E_f^2\left(V^2m^{-2}Hz^{-1}\right) = 3{V_a}^2/h^2. \tag{11}$$

The radio spectral flux density S_f in the isotropic plasma of refractive index $\mu = (1 - f_p^2/f^2)^{1/2}$ surrounding the antenna, can be expressed [e.g., *Deschamps*, 1962] by

$$S_f\left(Wm^{-2}Hz^{-1}\right) = \frac{E_f^2}{Z} = \mu\frac{3{V_a}^2}{Z_0h^2}, \tag{12}$$

where $Z(\Omega) = Z_0/\mu$ is the intrinsic impedance of the plasma, and $Z_0 = 1/\epsilon_0c = 120\,\pi \simeq 377\ \Omega$ in vacuo with permittivity ϵ_0 and speed of light c.

[50] Finally, the brightness temperature T_b of the type II radio emission in the plasma can be estimated from S_f, using the Rayleigh-Jeans radiation law

$$T_b(K) = \frac{\lambda^2}{2k_B}\frac{S_f}{\Delta\Omega} = \frac{c^2}{2k_B}\frac{3V_a^2}{Z_0h^2}\frac{1}{\mu f^2}\frac{1}{\Delta\Omega}, \tag{13}$$

Figure 4. Typical radio spectra taken at 128-s full time resolution around the shock passage between 1800 UT on 9 May 2001 and 0400 UT on 10 May 2001. Observed averaged voltage power spectrum (V^2 Hz^{-1} at receiver, black dotted lines); nonaveraged data (solid black lines) are superposed on 2-s averaged data to trace out any bursty plasma activity. Theoretical thermal noise spectrum fitted to observation (V^2 Hz^{-1} at receiver, red lines); radio emission spectrum above thermal noise background (V^2 Hz^{-1} at antenna, blue dotted lines). Spectrum 5 starting at 0034:39 UT and spanning the shock crossing at 0035:55 UT around 30 kHz: (left) before crossing, thermal noise spectrum for upstream region; (right) after crossing, for downstream. The sudden increase in the spectrum intensity around 30 kHz at the shock crossing is due to the increase of the thermal noise background in the downstream region.

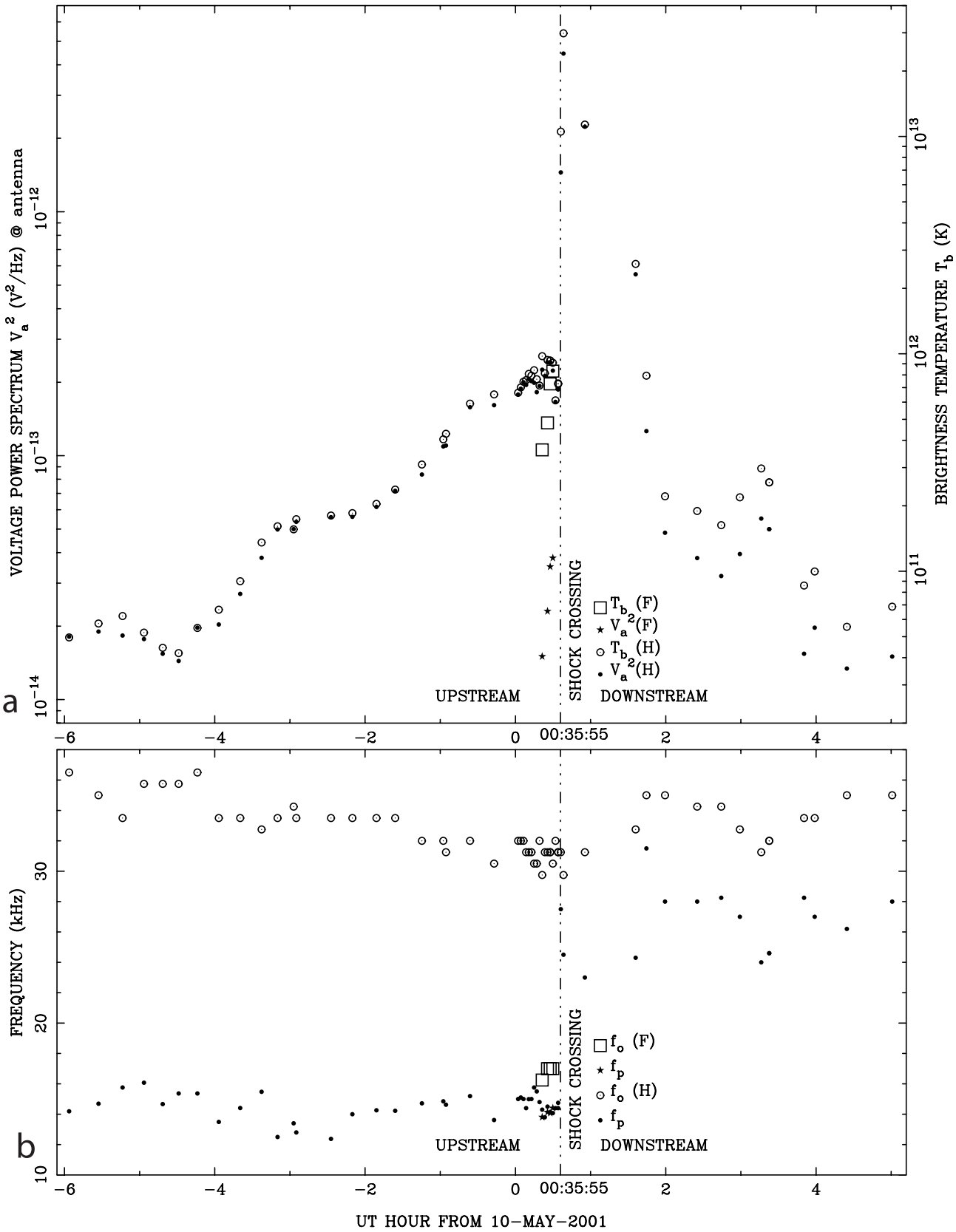

Figure 5. V_a^2 and T_b data for the type II emission observed in the same interval as Figure 4. (a) Voltage spectral density V_a^2(V^2 Hz^{-1}) measured at antenna for fundamental emission (star) and harmonic (dot). Brightness temperature $T_b(K)$ for fundamental (square) and harmonic (circled dot). (b) Plasma frequency f_p (kHz) measured at the time of fundamental emission (star) and harmonic (dot) observation. Observing frequency f_0 (kHz) for fundamental (square) and harmonic (circled dot).

where $\lambda = c/\mu f$ is the radiation wavelength in the plasma, k_B is the Boltzmann's constant, and $\Delta\Omega$ is the solid angle of the radio source. To deduce T_b, we use $h = 35$ m for the dipole antenna electrical length on Ulysses and take $\Delta\Omega = 2\pi$ for the solid angle of the type II kilometric emission (no spin modulation observed, hence extended source). The values of V_a^2 and T_b for the observed type II emission are then plotted in Figure 5a as functions of time, for the 10-hour interval spanning the shock crossing, together with the plasma frequency f_p and the observing frequency f_0 measured at the time of the spectral emission intensity peak (Figure 5b).

[51] Referring to Figure 5b, f_p varies between 12 and 16 kHz upstream; at the shock crossing it rises up rapidly to higher values and remains at values ranging between 24 and 30 kHz downstream. The harmonic f_0 data show a gradual decrease upstream, from about 36 kHz at the beginning of the interval, to 30 kHz at the approach of the shock; downstream, they remain at values fluctuating between about 30 and 35 kHz. Upstream, the ratio f_0/f_p is close to 2, especially near the passage of the shock; downstream, in contrast, there is no relationships between f_0 and f_p. These facts confirm the upstream origin of the type II source region, as evidenced by observation 1 described in section 4.

[52] From Figure 5a the harmonic V_a^2 and T_b data show a very similar general behavior through the interval of observation: from the beginning a steep rise up to the shock ramp, a peak value just after the shock crossing, then a rapid fall down to a low value at the end of the interval. Just before the crossing, the harmonic T_b is near 10^{12} K while the fundamental T_b is somewhat lower, at about 8×10^{11} K. The peak value of the harmonic T_b just after the crossing is $\simeq 3 \times 10^{13}$ K. This implies that at the shock crossing the s/c is at the closest approach of the type II source region, and the harmonic emission can be seen through the shock from downstream as far as the local f_p is lower than the observing frequency f_o.

[53] As can be seen in Figure 5a, there seems to exist a slight modulation with a periodicity of a few hours on both the harmonic V_a^2 and T_b data; it is clearer on the upstream leg than on the downstream leg after the crossing. The f_p and f_0 data seem also to be modulated, as shown in Figure 5b, but at a lesser extent and in anticorrelation with the V_a^2 and T_b modulation. The reason why the V_a^2 and T_b data are modulated is unknown.

7. Summary and Conclusion

[54] We have investigated the type II radio emission that is associated with the interplanetary CME-driven shock crossed on 10 May 2001 by Ulysses, then located at 1.35 AU near the ecliptic plane. This event is, to our knowledge, the unique case encountered until now by Ulysses since its 1990 launch, where the emission can be tracked all along its path in the IPM until the shock crossing and even after in the downstream region.

[55] The major results of the present study can be summarized as follows:

[56] 1. To track many patchy drifting features of the often very weak radio emission (of the order of the local plasma thermal noise) and automate their identification, we have used a computer code to characterize all local spectral emission peaks that appear in successive 30-min averaged spectra. The resulting peaks are then plotted on top of the spectrogram of the same data in the time t - inverse frequency $1/f$ coordinates. As the result of using $1/f$ as the ordinate, these peaks delineate many elongated clusters of points which highlight the type II emission on the spectrogram.

[57] 2. Least squares linear fits to identified clusters representative of the type II emission lead to straight lines of different slopes, which appear to converge to the same time at the Sun. Their analysis enables us to derive the speed and acceleration of the emitting shock, to know the radiation mode (fundamental or harmonic) of the emission cluster lines, and to determine the location and plasma density of the radio source regions along the shock front, using the corotating density measured continuously at the spacecraft.

[58] 3. The type II radio sources were found to be associated with corotating localized density variations of all scales encountered by the moving shock front. The relative variation of the densities in the radio sources are consistent with that found in the slopes of the fitted cluster lines, assuming the same constant shock speed. Their positions along the corotating density measured at the spacecraft could explain why the fundamental emission is usually not observed while the harmonic is not significantly affected.

[59] 4. The upstream boundary of the electron foreshock, where the type II radio emission takes place, was detected at least 42 s before the shock crossing, as evidenced by intense Langmuir waves occurring just above the local plasma frequency. This time interval yields a local shock curvature of 0.5×10^{-9} m^{-1} at most, or a curvature radius of 2×10^6 km at least. At the shock crossing, using the full time resolution data, we estimate the shock thickness to be less than 500 km.

[60] 5. The type II emission, observed during a 10-hour interval spanning the shock crossing, is analyzed in detail using the full time resolution spectrum data. We derive the plasma frequency and thermal noise background accurately from the thermal noise spectroscopy. This enables us to measure with accuracy the brightness temperature of the type II radio emission in the plasma surrounding the antenna. The brightness temperature of the harmonic emission shows a peak value of $\simeq 3 \times 10^{13}$ K just after the shock crossing. Just before the crossing, the harmonic temperature is near 10^{12} K and the fundamental temperature is somewhat lower, at about 8×10^{11} K.

[61] These brightness temperatures of the kilometric type II have been measured for the first time, to our knowledge, accurately and in well-identified conditions. Their theoretical interpretation will be forthcoming.

[62] **Acknowledgments.** The Ulysses/URAP experiment is a joint project of NASA/GSFC, the Observatoire de Paris, the University of Minnesota, and CETP, Velizy, France. The French contribution is supported by CNES and CNRS. Use was made of the SOHO/LASCO CME catalog which is generated and maintained at the CDAW Data Center by NASA and the Catholic University of America in cooperation with the Naval Research Laboratory. We thank Lidia Van Driel-Gesztelyi for her help in identifying the solar active region associated with the back-sided CME in this study. SH warmly thanks Michel Poquérusse for interesting discussions and his careful reading of an earlier manuscript.

[63] Amitava Bhattacharjee thanks the reviewers for their assistance in evaluating this paper.

References

Bale, S. D., M. J. Reiner, J.-L. Bougeret, M. L. Kaiser, S. Krucker, D. E. Larson, and R. P. Lin (1999), The source region of an interplanetary type II radio burst, *Geophys. Res. Lett.*, *26*, 1573.

Balogh, A., T. J. Beek, R. J. Forsyth, P. C. Hedgecock, R. J. Marquedant, E. J. Smith, D. J. Southwood, and B. T. Tsurutani (1992), The magnetic field investigation on the Ulysses mission: Instrumentation and preliminary scientific results, *Astron. Astrophys. Suppl.*, *92*, 221.

Bame, S. J., D. J. McComas, B. L. Barraclough, J. L. Phillips, K. J. Sofaly, J. C. Chavez, B. E. Goldstein, and R. K. Sakurai (1992), The Ulysses solar wind plasma experiment, *Astron. Astrophys. Suppl.*, *92*, 237.

Bougeret, J.-L. (1997), The heliospheric signatures of coronal mass ejections, in *Correlated Phenomena at the Sun, in the Heliosphere and in Geospace*, edited by A. Wilson, *Eur. Space Agency Spec. Publ.*, *ESA SP-415*, 523.

Bougeret, J.-L., et al. (1995), WAVES: The radio and plasma wave investigation on the WIND spacecraft, *Space Sci. Rev.*, *71*, 231.

Cane, H. V. (2000), ISEE-3 observations of radio emission from coronal and interplanetary shocks, in *Radio Astronomy at Long Wavelenths*, *Geophys. Monogr. Ser.*, vol. 119, edited by R. G. Stone et al., p. 147, AGU, Washington, D. C.

Deschamps, G. A. (1962), Impedance of an antenna in a conducting medium, *IEEE Trans. Ant. Propag.*, *AP10*, 648.

Dulk, G. A., Y. Leblanc, and J.-L. Bougeret (1999), Type II shock and CME from the corona to 1 AU, *Geophys. Res. Lett.*, *26*, 2331.

Fainberg, J., S. Hoang, and R. Manning (1985), Measurements of distributed polarized radio sources from spinning spacecraft; effect of a tilted axial antenna. ISEE-3 application and results, *Astron. Astrophys.*, *153*, 145.

Filbert, P. C., and P. J. Kellogg (1979), Electrostatic noise at the plasma frequency beyond the Earth's bow shock, *J. Geophys. Res.*, *84*, 1369.

Hoang, S., G. A. Dulk, and Y. Leblanc (1994), Interplanetary type III radio bursts that approach the plasma frequency: Ulysses observations, *Astron. Astrophys.*, *289*, 957.

Issautier, K., N. Meyer-Vernet, M. Moncuquet, and S. Hoang (1998), Solar wind radial and latitudinal structure: Electron density and core temperature from Ulysses thermal noise spectroscopy, *J. Geophys. Res.*, *103*, 1969.

Kellogg, P. J. (1980), Fundamental emission in three type III solar bursts, *Astrophys. J.*, *236*, 696.

Knock, S. A., I. H. Cairns, P. A. Robinson, and Z. Kuncic (2001), Theory of type II radio emission from the foreshock of an interplanetary shock, *J. Geophys. Res.*, *106*, 25,041.

Lacombe, C., C. C. Harvey, S. Hoang, A. Mangeney, J.-L. Steinberg, and D. Burgess (1988), ISEE observations of radiation at twice the solar wind plasma frequency, *Ann. Geophys.*, *6*, 113.

Lengyel-Frey, D. (1992), Location of the radio emitting regions of interplanetary shocks, *J. Geophys. Res.*, *97*, 1609.

Manning, R. (2000), Instrumentation for space-based low frequency radio astronomy, in *Radio Astronomy at Long Wavelenths*, *Geophys. Monogr. Ser.*, vol. 119, edited by R. G. Stone et al., p. 329, AGU, Washington, D. C.

Manning, R., and J. Fainberg (1980), A new method of measuring radio source parameters of a partially polarized distributed source from spacecraft observations, *Space Sci. Instrum.*, *5*, 161.

McComas, D. J., S. J. Bame, W. C. Feldman, J. T. Gosling, and J. L. Phillips (1992), Solar wind halo electrons from 1–4 AU, *Geophys. Res. Lett.*, *19*, 1291.

Meyer-Vernet, N., S. Hoang, K. Issautier, M. Moncuquet, and G. Marcos (2000), Plasma thermal noise: The long wavelength radio limit, in *Radio Astronomy at Long Wavelenths*, *Geophys. Monogr. Ser.*, vol. 119, edited by R. G. Stone et al., p. 67, AGU, Washington, D. C.

Poquérusse, M., S. Hoang, J.-L. Bougeret, and M. Moncuquet (1996), Ulysses-ARTEMIS radio observations of energetic flare electrons, in *Solar Wind Eight*, edited by D. Winterhalter et al., *AIP Conf. Proc.*, *382*, 62.

Reiner, M. J. (2000), Interplanetary type II radio emissions associated with CMEs, in *Radio Astronomy at Long Wavelenths*, *Geophys. Monogr. Ser.*, vol. 119, edited by R. G. Stone et al., p. 137, AGU, Washington, D. C.

Reiner, M. J., M. L. Kaiser, J. Fainberg, J.-L. Bougeret, and R. G. Stone (1998a), On the origin of radio emissions associated with the January 6–11, 1997 CME, *Geophys. Res. Lett.*, *25*, 2493.

Reiner, M. J., M. L. Kaiser, J. Fainberg, and R. G. Stone (1998b), A new method for studying remote type II radio emissions from coronal mass ejection-driven shocks, *J. Geophys. Res.*, *103*, 29,651.

Stone, R. G., et al. (1992), The unified radio and plasma wave investigation on Ulysses, *Astron. Astrophys. Suppl.*, *92*, 291–316.

S. Hoang and C. Lacombe, Laboratoire d'Etudes Spatiales et d'Instrumentation en Astrophysique, Observatoire de Paris, UMR 8109 CNRS, F-92195 Meudon, France. (sang.hoang@obspm.fr; catherine.lacombe@obspm.fr)

R. J. MacDowall, NASA Goddard Space Flight Center, Greenbelt, MD 20895, USA. (robert.macdowall@nasa.gov)

G. Thejappa, Department of Astronomy, University of Maryland, College Park, MD 20742, USA. (golla@gsfc.nasa.gov)